Base-type-selective high-resolution ^{13}C edited NOESY for sequential assignment of large RNAs

Bernhard Brutscher[a], Jérôme Boisbouvier[a], Eriks Kupče[b], Carine Tisné[c], Frédéric Dardel[c], Dominique Marion[a] & Jean-Pierre Simorre[a,*]

[a]*Institut de Biologie Structurale – Jean-Pierre Ebel, C.N.R.S.-C.E.A., 41 rue Jules Horowitz, F-38027 Grenoble Cedex, France;* [b]*Varian Inc., 28 Manor Rd., Walton-on-Thames, Surrey KT12 2QF, U.K.;* [c]*Université Paris V, 4 avenue de l'observatoire, F-75270 Paris, France*

Abstract

Extensive spectral overlap presents a major problem for the NMR study of large RNAs. Here we present NMR techniques for resolution enhancement and spectral simplification of fully ^{13}C labelled RNA. High-resolution ^{1}H-^{13}C correlation spectra are obtained by combining TROSY-type experiments with multiple-band-selective homonuclear ^{13}C decoupling. An additional C-C filter sequence performs base-type-selective spectral editing. Signal loss during the filter is significantly reduced because of TROSY-type spin evolution. These tools can be inserted in any ^{13}C-edited multidimensional NMR experiment. As an example we have chosen the ^{13}C-edited NOESY which is a crucial experiment for sequential resonance assignment of RNA. Application to a 33-nucleotide RNA aptamer and a 76-nucleotide tRNA illustrates the potential of this new methodology.

Introduction

The availability of methods for isotope (^{13}C, ^{15}N, and ^{2}H) labelling of RNA and the development of novel heteronuclear NMR experiments have allowed the characterisation of three-dimensional structures of a large number of RNAs in the past 10 years (Batey et al., 1992; Nikonowicz and Pardi, 1993; Varani et al., 1996; Wijmenga and van Buren, 1998). Despite these advances, only RNA with a molecular weight less than about 15 kDa ($\approx$44 nucleotides) is currently accessible to NMR studies. A major problem for the study of larger RNAs is the low chemical shift dispersion, resulting in extensive resonance overlap in the multidimensional correlation spectra. Since many biologically interesting RNAs are significantly larger than 15 kDa, it is important to develop techniques for resolution enhancement and spectral simplification that

will make these molecules accessible to solution state NMR spectroscopy.

Resonance assignment of fully ^{13}C/^{15}N-labelled RNA is mainly based on a set of heteronuclear through-bond transfer experiments correlating the nuclear spins within the same sugar, the same base, or between sugar and base of the same nucleotide (Pardi and Nikonowicz, 1992; Simorre et al., 1995, 1996; Fiala et al., 1998, 2000). For large RNAs, however, the inter-nucleotide through-bond correlation experiment HCP (Marino et al., 1995; Varani et al., 1995) becomes very inefficient, and sequential resonance assignment requires the detection of ^{1}H-^{1}H NOEs between the sugar protons H$_{1'}$ and the aromatic base protons, H$_6$ or H$_8$ of sequential nucleotides. The ^{13}C edited NOESY is therefore a crucial experiment for study of RNA by NMR. With increasing size of the RNA the interpretation of ^{13}C edited NOESY spectra becomes difficult because of overlapping resonances, increased line widths, and carbon-carbon-coupling-induced line
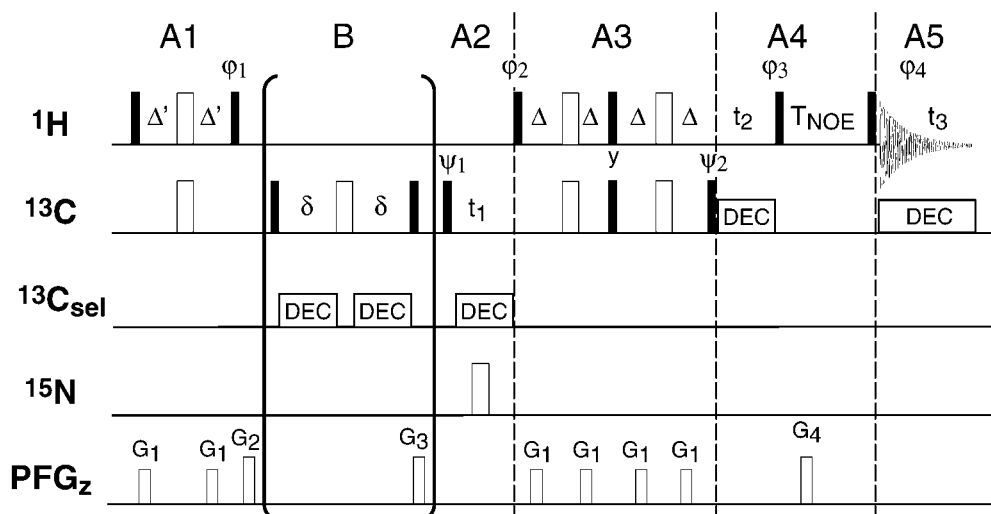
Figure 1. (A) TROSY-NOESY pulse sequence for recording 3D ^{13}C edited NOESY spectra on fully ^{13}C labelled RNA, and (B) optional base-type selective C-C filter sequence. Thin bars represent 90° and open bars 180° RF pulses. Composite ^{13}C 180° pulses are used for broadband spin inversion (90°_x 240°_y 90°_x) and refocusing (59.4°_x 298°_{-x} 59.4°_x). All pulses are applied along the x axis unless indicated. The transfer delays Δ and Δ' are adjusted to $1/4J_{CH}$, taking into account the different relaxation times of the involved coherences. In the present case they were set to $\Delta = 1.3$ ms and $\Delta' = 1.0$ ms. The filter delay δ was set to $\delta = 1/2J_{C_5C_6} = 7.5$ ms. The recycle delay between experiments was optimised experimentally and set to 1.5 s. Heteronuclear ^{13}C decoupling was achieved using GARP with an RF field strength of $|\gamma B_1|/2\pi = 3$ kHz. Homonuclear band-selective ^{13}C decoupling was realised by a train of adiabatic WURST-2 pulses as described in the text. Pulsed field gradients along the z-axis (PFG$_z$) were applied as indicated for coherence transfer pathway selection. The gradient strength was approximately 50 G/cm, and the pulse lengths (G$_1$, G$_2$, G$_3$, G$_4$) were set to different values ranging from 100 µs to 900 µs, followed by a recovery delay of 300 µs. The phase φ_1 is adjusted to enhance the slowly relaxing C^+H^β coherence (Brutscher et al., 1998). The sign of $\varphi_1 = \pm y$ depends on the spectrometer phase convention, and should thus be determined experimentally. Echo/anti-echo quadrature detection in t_1 is obtained by recording two experiments E$_1$ and E$_2$ with the following phase settings: E$_1$: $\varphi_2 = 4y$; $\varphi_3 = 2x,2y$; $\varphi_4 = 2(x,-x)$; $\psi_1 = x,-x,-y,y$; $\psi_2 = 4x$; and E$_2$: $\varphi_2 = 4(-y)$; $\varphi_3 = 2x,2(-y)$; $\varphi_4 = 2(x,-x)$; $\psi_1 = x,-x,-y,y$; $\psi_2 = 4(-x)$. They are then combined as usual for echo/anti-echo detection to reconstruct the real and imaginary part of the NMR signal in t_1. 2D ^{1}H-^{13}C correlation spectra without NOE mixing are recorded by omitting the pulse element A4 and changing phase φ_4 to $\varphi_4 = x,-x,y,-y$ for E$_1$, and $\varphi_4 = x,-x,-y,y$ for E$_2$. For quadrature detection in t_2, time proportional phase incrementation of φ_3 is applied according to STATES-TPPI. If the C-C filter (B) is added, two data sets are recorded with and without C$_5$-band decoupling during the filter delays δ in an interleaved manner. During processing the two data sets are added and subtracted to obtain the desired sub-spectra as explained in the text.

splitting in the ^{13}C dimension. In order to simplify the spectra, selective ^{2}H or ^{13}C labelling at specific positions in the RNA sugars and bases, or of specific nucleotides has been used advantageously in the past (Tolbert and Williamson, 1996; Dieckman and Feigon, 1997; Nikonowicz et al., 1998). These biochemical methods, however, are both costly and time consuming, as several RNA samples have to be prepared by chemical and enzymatic synthesis using different labels. An attractive alternative is the development of novel NMR tools which provide the desired high spectral resolution. In the last three years, experimental techniques for resolution and sensitivity enhancement of heteronuclear correlation spectra have been developed, which make use of the favourable relaxation properties of single-transition spin states. Such techniques have become widely known as transverse relaxation optimised spectroscopy (TROSY) (Pervushin et al., 1997, 1998; Czish and Boelens, 1998; Weigelt, 1998; Cordier et al., 1999; Brutscher, 2000). Recently, we have shown that the resolution of ^{13}C edited NOESY spectra can be substantially improved by using TROSY combined with low-level (10–20%) ^{13}C enrichment of the RNA (Brutscher et al., 1998). Here we will show that spectra of comparable resolution, but with considerably increased sensitivity can be obtained for fully ^{13}C/^{15}N labelled RNA. ^{13}C line splitting due to scalar carbon-carbon couplings is removed using band-selective homonuclear ^{13}C decoupling. An additional C-C filter sequence allows recording of base-type selective ^{13}C edited NOESY spectra without the need of specifically isotope labelled RNA samples. Application to a 33-nucleotide RNA aptamer and a 76-nucleotide tRNA$_3^{\text{Lys}}$ illustrates the important gain in spectral resolution achieved by this new method.

Materials and methods

3D TROSY-NOESY experiment designed for fully ^{13}C, ^{15}N labelled RNA

The pulse scheme employed for the 3D ^{13}C edited NOESY experiment is shown in Figure 1 (inserts A1–A5). In short, the coherence transfer pathway during the pulse sequence is as follows: after an initial INEPT step (A1) which transfers ^1H magnetisation into two-spin order $2C_zH_z$, the ^{13}C spins are frequency labelled during t_1 (A2) while removing homonuclear carbon-carbon scalar couplings as explained in the following section. No ^1H decoupling is applied to avoid inter-conversion of the H^α and H^β spin states during t_1, which is the basic principle of TROSY. The slowly relaxing ^{13}C doublet line is selected by the sequence block A3 which performs spin-state-selective coherence transfer from ^{13}C to ^1H (Pervushin et al., 1997; Sørensen et al., 1997). Following the sign convention of Brutscher et al. (1998), this transfer is described by $C^+H^\beta \rightarrow C^\alpha H^+$. The ^1H spins are then frequency labelled during t_2 followed by a NOESY mixing period (A4). The ^{13}C spins are decoupled during t_2 as no significant resolution enhancement is expected from TROSY-type spin evolution of the carbon-bound protons (Brutscher et al., 1998). In addition, scalar coupling evolution between base carbons and nitrogens is removed by a 180° RF pulse applied to the ^{15}N spins at time $t_1/2$. In the final step (A5), the ^1H free induction decay (FID) is detected while decoupling ^{13}C. The pulse scheme includes the now common features of simultaneous use of ^1H and ^{13}C steady state magnetisation and sensitivity enhanced quadrature detection in t_1 (Brutscher et al., 1998; Pervushin et al., 1998). The H_i-H_j NOE cross peaks are detected in the final 3D spectrum at $(\nu_1, \nu_2, \nu_3) = (\nu_{C_i} + J_{CH}/2, \nu_{H_i}, \nu_{H_j})$. Base-type selective ^{13}C edited NOESY spectra are obtained by adding the C-C filter element (insert B) to the experiment as explained in more detail later on. The 2D ^1H-^{13}C correlation spectra shown in this article were recorded by omitting the sequence block labelled A4 and adjusting the phase cycle as explained in the figure caption.

Multiple-band-selective homonuclear ^{13}C decoupling

To achieve high resolution in the ribose $C_{1'}$ and the aromatic C_6, C_8 carbon spectral regions, the one-bond scalar couplings $^1J_{C_{1'}C_{2'}} \cong 43$ Hz and $^1J_{C_5C_6} \cong 67$ Hz (Wijmenga and van Buren, 1998) were removed by homonuclear ^{13}C decoupling applied simultaneously to the C_5 and $C_{2'}$ frequency bands. Additional decou-

pling of the low-field aromatic carbon region helps reducing modulation side-bands and removes long-range scalar couplings between the aromatic C_6 and C_8 carbons in purines, $J_{C_6C_8} \cong 9$ Hz (Wijmenga and van Buren, 1998). The ^{13}C frequency bands of the different sugar and base carbons are shown in Figure 2. Band-selective homonuclear ^{13}C decoupling during ^{13}C frequency labelling (t_1) and the C-C filter was experimentally realised by a train of adiabatic WURST-2 inversion pulses (Kupče and Freeman, 1996). The decoupling sequence was initiated at the beginning of the t_1-period and simply truncated at the end of t_1. Adiabatic decoupling was chosen for its weak off-resonance irradiation, which is very important in the present application as the detected $C_{1'}$ and the decoupled C_5 bands are only about 1 ppm apart. For optimal decoupling performance a WURST pulse length of $T_P \leq 1/5 J_{CC}$ has to be chosen. For the applications presented here T_P was set to 3.0 ms and an adiabaticity factor of $Q = 2.0$ was used for all decoupling bands. The steepness of the transition regions in the decoupling profile depends primarily on the T_P and hence on J_{CC}. Obviously, a high magnetic field strength providing a better separation between the decoupled and the observed regions is beneficial in such experiments. The WURST waveforms were calculated to cover bandwidths of 16 ppm centred at 72 ppm for the $C_{2'}$ band, 105 ppm for the C_5 band of pyrimidines, and 160 ppm for the low-field aromatic carbon region. Note that the so defined $C_{2'}$ band also covers the $C_{3'}$ and most of the $C_{5'}$ resonances (Figure 2). The waveforms were then superposed (Kupče and Freeman, 1993) and phase cycled according to the TPG-5 supercycle (Tycko et al., 1985). Opposite sense frequency sweeps (Zhang and Gorenstein, 1998) were used for the different WURST waveforms to reduce the Bloch–Siegert shifts and appearance of modulation side-bands. Simulations showing the decoupling profiles of WURST-2 waveforms used in this work are available upon request.

Base-type-selective spectral editing using C-C filters

The spectral editing filter sequence of Figure 1B makes use of the different ^{13}C-^{13}C coupling topologies in RNA bases to separate the resonances from C_8 in purines and C_6 in pyrimidines (Pur/Pyr-filter). For maximum filter efficiency the filter delay δ has to be adjusted to $\delta = 1/2 J_{C_5C_6}$. Two separate experiments are recorded, (I) with and (II) without decoupling of the C_5 band during the filter. Spin evolution during the C-C filter is described as $C_8^+ H_8^\beta \rightarrow C_8^+ H_8^\beta$ for
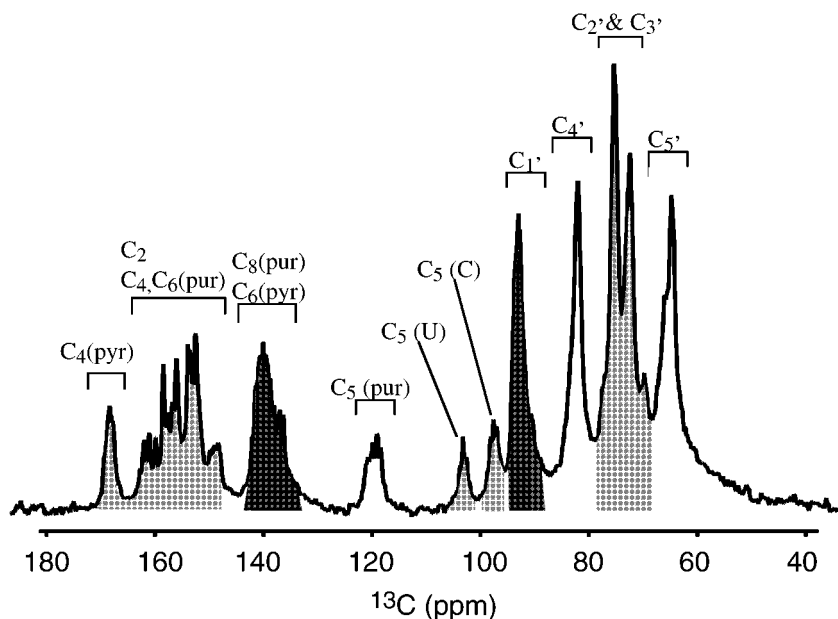
Figure 2. ^{13}C spectrum of the 33-nucleotide theophylline-binding RNA aptamer. Ten frequency bands can be distinguished which correspond to chemically different carbon sites in the ribose and the bases. The frequency bands to be observed (C_6/C_8, and $C_{1'}$) and decoupled (C_5, $C_{2'}/C_{3'}$, and low-field aromatic carbons) are highlighted by filled and lined regions in the spectrum.

purines, and $C_6^+ H_6^\beta \rightarrow \pm C_6^+ H_6^\beta$ for pyrimidines. During data processing the two experiments are either added or subtracted to yield the purine and pyrimidine spectra, respectively. Additional $C_{2'}$ and low-field aromatic carbon decoupling during the C-C filter in both experiments (I) and (II) is applied for maximal sensitivity in the $C_{1'}$ and C_8 spectral regions. $C_{1'}$ spin evolution during the C-C filter is then given by $C_{1'}^+ H_{1'}^\beta \rightarrow C_{1'}^+ H_{1'}^\beta$, and the corresponding correlation peaks are detected together with the purine base correlations in the sum spectrum. The same filter sequence can also be used to separate the resonances from uridine (Uri) and cytidine (Cyt) bases in two different spectra (Cyt/Uri-filter). By limiting the selective decoupling to the C_5(Uri) band (see Figure 2), spin evolution during the filter is given by $C_8^+ H_8^\beta \rightarrow C_8^+ H_8^\beta$ for purine, $C_6^+ H_6^\beta \rightarrow -C_6^+ H_6^\beta$ for cytidine, and $C_6^+ H_6^\beta \rightarrow \pm C_6^+ H_6^\beta$ for uridine bases. Using this Cyt/Uri-filter, only the C_6 of uridine are detected in the difference spectrum whereas the C_6 of cytidine are now present in the sum spectrum with opposite sign with respect to the purine C_8, and the ribose $C_{1'}$ resonances. For the Pur/Pyr filter the same composite WURST waveform was used as for the ^{13}C band-selective decoupling during t_1. For the Uri/Cyt filter the centre of the C_5 decoupling band was shifted to

111 ppm without changing the bandwidth of 16 ppm. Bloch-Siegert phase shifts during the C-C filter are refocused by the 180° ^{13}C pulse.

Experimental conditions

Multiple-band-selective homonuclear ^{13}C decoupling, base-type-selective spectral editing, and 3D TROSY-NOESY are demonstrated here on two fully ^{13}C/^{15}N labelled RNA samples: a 33-nucleotide RNA aptamer (Figure 6) in a 1:1 complex with unlabelled theophylline dissolved in a buffer of 20 mM sodium phosphate (pH 6.8), 30 mM NaCl, 2 mM MgCl$_2$ in D$_2$O (Zimmermann et al., 1997), and a 76-nucleotide tRNA$_3^{Lys}$ (Figure 7A) prepared in a phosphate buffer, dialysed against water and lyophilised, and then dissolved in D$_2$O at pH = 5.6 (Tisné et al., 2000). Both RNA samples were prepared at about 1 mM concentration. All data were recorded on a Varian INOVA 800 spectrometer equipped with a triple-resonance probe and shielded pulsed field gradients (PFG). The sample temperature was set to 25 °C for the theophylline-binding RNA aptamer. A higher temperature of 45 °C was chosen for the tRNA$_3^{Lys}$ corresponding to the optimal conditions for an NMR study of this RNA. ^{1}H-^{13}C correlation spectra were recorded with 1024 (^{1}H) × 300 (^{13}C) complex points, and spectral widths of 12 ppm (^{1}H) and 50 ppm (^{13}C). The total acqui-
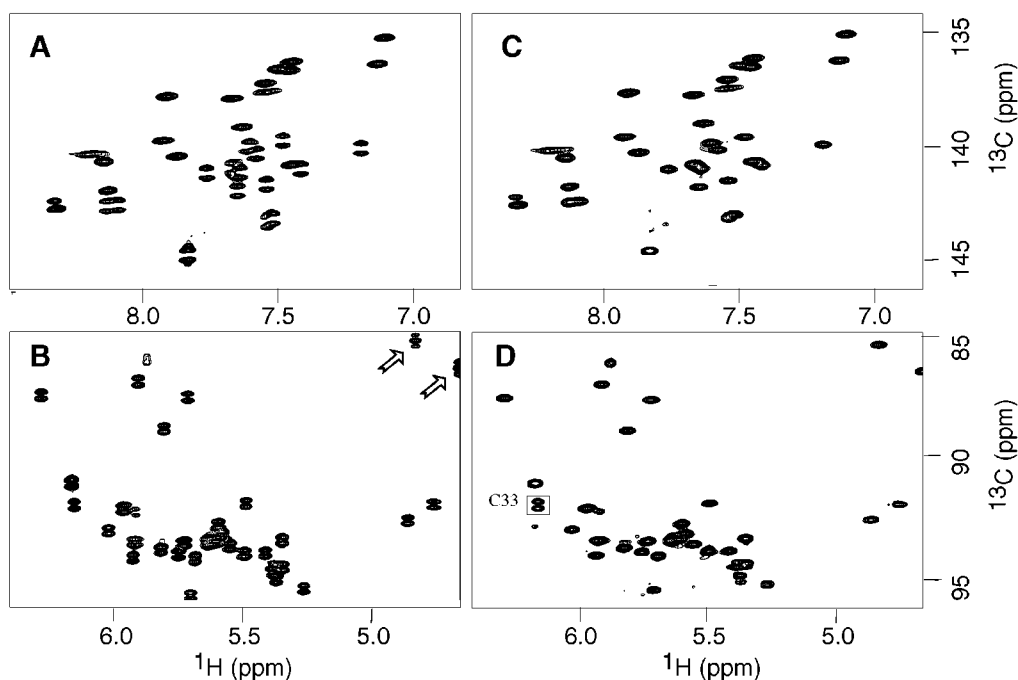
Figure 3. ^{1}H-^{13}C TROSY correlation spectra of the 33-nucleotide theophylline-binding RNA aptamer recorded without (A and B), and with (C and D) homonuclear multiple-band-selective ^{13}C decoupling. Only the spectral regions corresponding to C_6-H_6 and C_8-H_8 (A and C) and to $C_{1'}$-$H_{1'}$ (B and D) are plotted. The two triplet peaks in (B) highlighted by an arrow correspond to $C_{4'}$-$H_{4'}$ correlations of U23 and C27 which are also decoupled from $C_{3'}$ and $C_{5'}$ by the WURST pulse train (D).

sition time was 2 h for the RNA aptamer, and 5 h for the tRNA$_3^{\text{Lys}}$. For the 3D TROSY-NOESY experiment data sets of 128 (ω_1) × 40 (ω_2) × 512 (ω_3) complex points were acquired for spectral widths of 30 ppm ($\omega_1 = {}^{13}$C), 7.5 ppm ($\omega_2 = {}^1$H), and 12 ppm ($\omega_3 = {}^1$H). The NOESY mixing time was set to $T_{\text{NOE}} = 200$ ms (RNA aptamer) and $T_{\text{NOE}} = 120$ ms (tRNA$_3^{\text{Lys}}$). The experimental times were 68 h and 100 h for the RNA aptamer and the tRNA$_3^{\text{Lys}}$, respectively. Processing of NMR data was achieved using the FELIX program version 98.0 (Molecular Simulations Inc.). After signal apodisation using squared cosine functions, the time-domain data were Fourier transformed to final matrices of 2048 (ω_1) × 1024 (ω_3) data points for the 2D TROSY spectra and 256 (ω_1) × 128 (ω_2) × 512 (ω_3) for the 3D TROSY-NOESY spectra.

Results and discussion

High resolution ^{1}H-^{13}C 2D TROSY and 3D TROSY-NOESY of fully ^{13}C,^{15}N labelled RNA

In Figures 3A and 3B are plotted the spectral regions of a ^{1}H-^{13}C TROSY-type correlation spectrum recorded on the 33-nucleotide RNA aptamer comprising the C_6-H_6 and C_8-H_8, and $C_{1'}$-$H_{1'}$ correlation peaks, respectively. TROSY spectra were obtained for this fully ^{13}C/^{15}N labelled RNA sample without artefact and with a significant gain in spectral resolution and sensitivity with respect to a HSQC-type spectrum (data not shown). Compared to a previously recorded ^{1}H-^{13}C TROSY on a 15% ^{13}C labelled RNA sample (Brutscher et al., 1998), spectral resolution is limited by the appearance of line splitting due to one-bond carbon-carbon couplings. A well known technique to remove these line splittings is constant time (CT) frequency editing (Bax et al., 1979). The large scattering in the coupling constants ($^1J_{C_{1'}C_{2'}} \cong 43$ Hz in the ribose and $^1J_{C_5C_6} \cong 67$ Hz in the pyrimidine bases), the important loss of signal during the CT delay $T = 1/J_{\text{CC}}$, and the limited acquisition time ($t_1^{\text{max}} \leq 1/J_{\text{CC}}$), however, make this approach impractical for
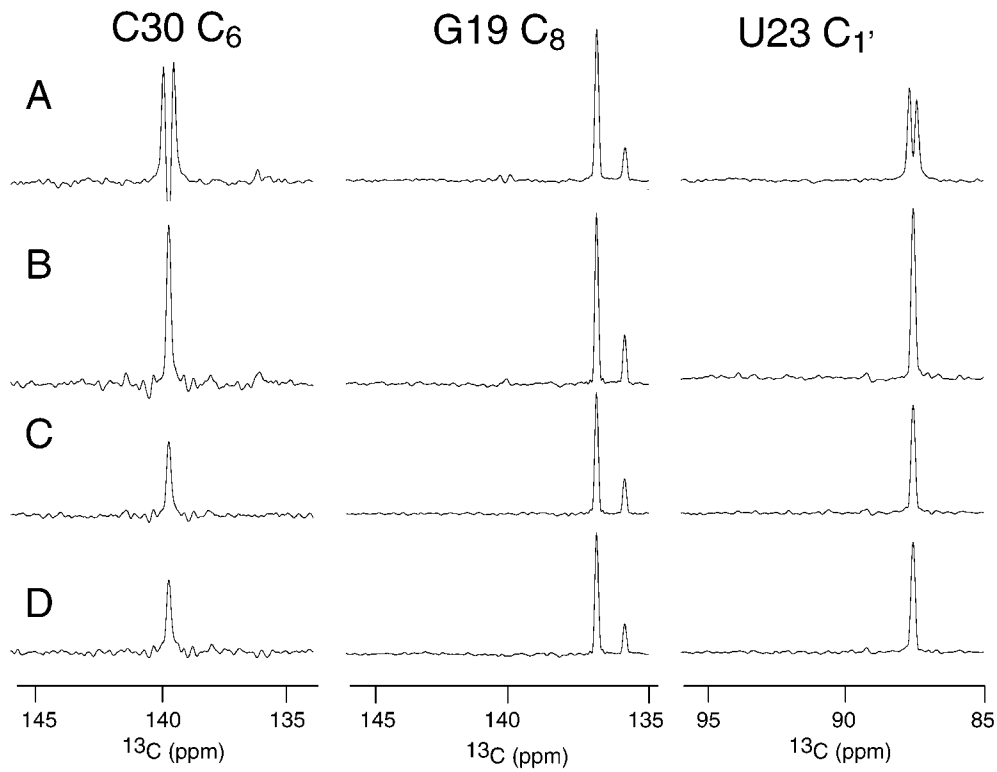
Figure 4. 1D ^{13}C traces extracted from ^{1}H-^{13}C TROSY spectra of C_6 (C30), C_8 (G19), and $C_{1'}$ (U23) of the 33-nucleotide RNA aptamer recorded (A) without ^{13}C decoupling and C-C filter, (B and D) with homonuclear decoupling of the C_5, $C_{2'}$, and low-field aromatic carbon bands, (C) with additional Pyr/Pur-filter, and (D) with additional Cyt/Uri-filter.
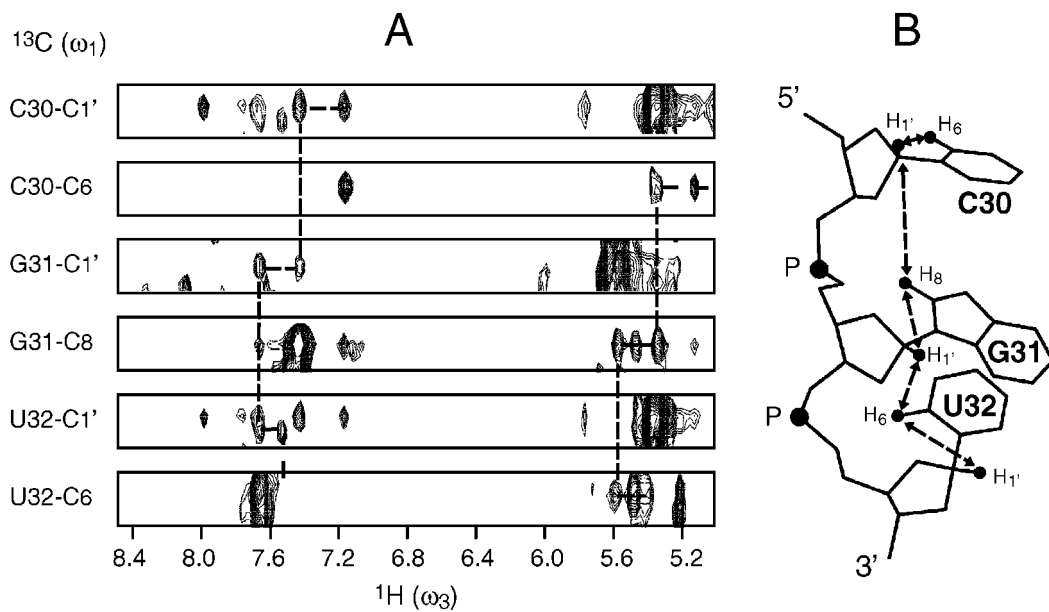

Figure 5. (A) 2D NOE strips ($\omega_1 = {}^{13}$C, $\omega_3 = {}^1$H) of a 3D ^{13}C edited TROSY-NOESY spectrum recorded on the 33-nucleotide RNA aptamer with the pulse sequence of Figure 1A. Intra-nucleotide and sequential NOEs required for resonance assignment are connected by dashed lines in the spectra. (B) Sequential assignment pathway in the corresponding C30-G31-U32 base sequence.
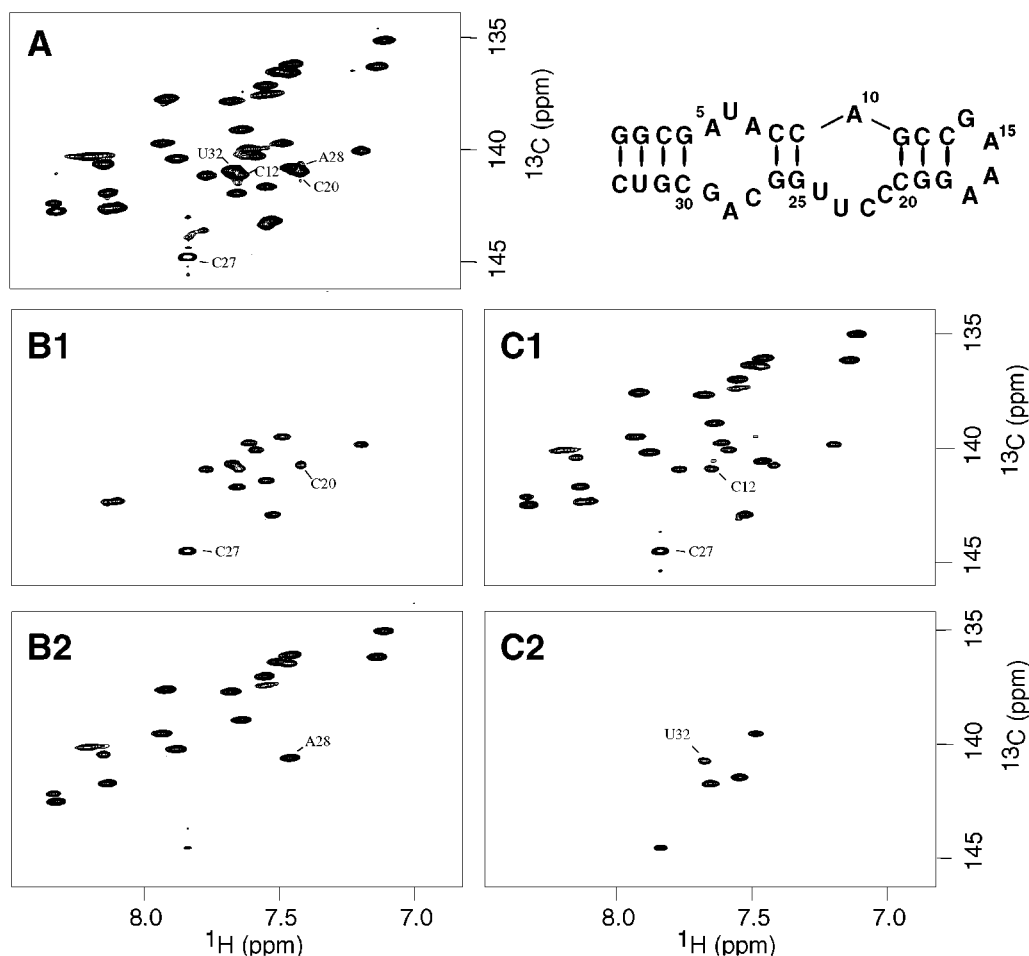
Figure 6. Base region of a ^{1}H-^{13}C correlation spectrum of the 33-nucleotide RNA aptamer recorded with the pulse sequence of Figure 1 using multiple-band-selective ^{13}C decoupling (A), and an additional Pyr/Pur filter (B1 and B2), or an additional Cyt/Uri filter (C1 and C2). For a fair comparison of the spectral resolution the contour levels in the spectra B and C are scaled by a factor of 0.6 corresponding to the average sensitivity difference. For the most intense C27 line labelled in spectra B1 and C1, residual peaks are observed at the same frequencies in spectra B2 and C2 and their relative intensities are below 5 and 8 % of the correctly filter peaks, respectively. The secondary structure of the 33-nucleotide theophylline-binding RNA aptamer is drawn in the upper right corner.

studies of larger RNAs. An interesting feature of RNA is that the ^{13}C spectrum splits into many distinct spectral regions (bands) corresponding to the chemically different carbon sites. These bands have little overlap, as illustrated in Figure 2. Therefore if one is mainly interested in certain parts of the ^{13}C spectrum, an attractive alternative to CT frequency editing relies on band-selective homonuclear decoupling (McCoy and Mueller, 1992; Kupče et al., 1999). The ^{13}C frequency bands are only little influenced by the tertiary structure of the RNA (or DNA) and band-selective homonuclear ^{13}C decoupling should therefore be applicable to most nucleic acids. In the context of NOE-based sequential assignment, simultaneous decoupling of the $C_{2'}$ and

C_5 bands applied during the ^{13}C frequency labelling period removes the line splittings in the ^{13}C spectrum. A ^{1}H-^{13}C correlation spectrum recorded using the pulse sequence of Figure 1 (inserts A1, A2, A3, and A5) is shown in Figures 3C (C_6-H_6 and C_8-H_8 regions) and 3D ($C_{1'}$-$H_{1'}$ region). One observes that the adiabatic WURST pulse train decouples the C_5 band without notably affecting the resonances of the nearby $C_{1'}$ band (see Figure 2). Simultaneously the line splittings in the $C_{1'}$ carbon spectrum are removed except for the $C_{3'}$-terminal nucleotide C33. For this ribose the $C_{2'}$ resonance is about 10 ppm outside the normal range for $C_{2'}$. The band-selective ^{13}C decoupling also enhances resolution in the $C_{4'}$ sugar carbon spectral
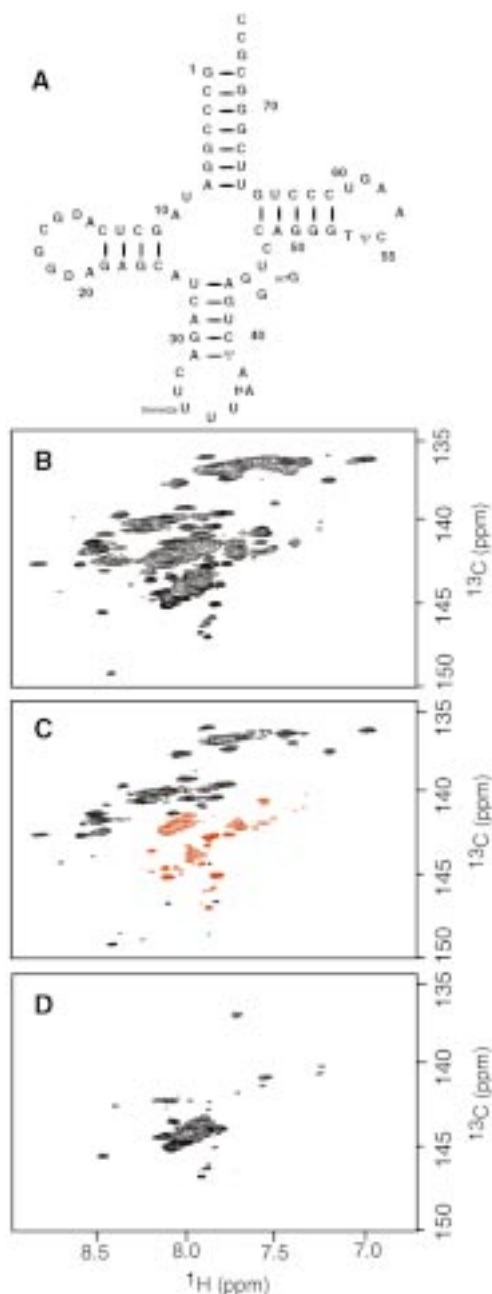
148

Figure 7. (A) Secondary structure of the 76-nucleotide tRNA$_3^{Lys}$. (B) Base region of a ^{1}H-^{13}C correlation spectrum of tRNA$_3^{Lys}$ recorded with the pulse sequence of Figure 1A using multiple-band-selective ^{13}C decoupling. The same regions of a ^{1}H-^{13}C correlation spectrum recorded with an additional Cyt/Uri filter are shown in (C) the sum spectrum, and (D) the difference spectrum. The red-coloured contours in (C) correspond to negative cross peak intensities which can be assigned to cytidine resonances. The cross peaks in (D) can be assigned to uridine resonances. For a fair comparison of the spectral resolution the contour levels of (C) and (D) are scaled by a factor of 0.6.
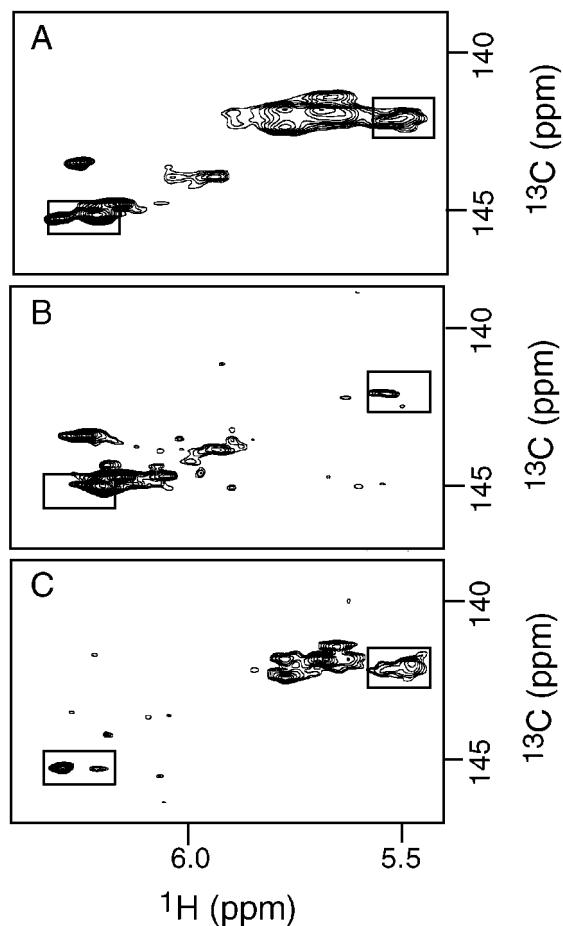

Figure 8. 2D strips extracted from 3D ^{13}C-edited TROSY-NOESY spectra of tRNA$_3^{Lys}$ recorded with the pulse sequence of Figure 1 using multiple-band-selective ^{13}C decoupling (A), and an additional Cyt/Uri filter (B and C). The three 2D strips were extracted at a ^{1}H frequency ω_2 = 8.05 ppm corresponding to several overlapping H$_6$ pyrimidine resonances. The contour levels in the sum (B) and difference (C) spectra are scaled by a factor of 0.6. Spectral regions with overlapping NOE cross peaks which can be separated by the Cyt/Uri filter are highlighted by boxes.

region, as the C$_{3'}$ and C$_{5'}$ bands are affected by the ^{13}C decoupling (see Figure 2). Therefore most $J_{C_{3'}C_{4'}}$ and $J_{C_{4'}C_{5'}}$ scalar coupling-induced line splittings are removed, as demonstrated for nucleotides U23 and C27 in Figure 3 where the C$_{4'}$ triplet lines detected in the non-decoupled TROSY spectrum (Figure 3B) collapse to singlet lines in the decoupled spectrum (Figure 3D).

The performance of the homonuclear ^{13}C decoupling is best appreciated from 1D traces along the ^{13}C dimension, as shown for representative examples in Figures 4A and 4B for TROSY spectra with and without homonuclear ^{13}C decoupling, respectively. For the

experimental conditions chosen here, the sensitivity gain in the C_5 and $C_{2'}$-decoupled spectrum with respect to the non-decoupled spectrum is about 2.0 for the $C_{1'}$ and 1.5–1.8 for the C_6 carbons. These results show that the decoupling performance of the WURST sequence is close to optimal for both frequency bands. Additional WURST decoupling of the low-field aromatic carbons leads to a slight enhancement ($\approx 10\%$) of the C_8 singlet by the cancellation of the unresolved $^3J_{C_6C_8}$. A drawback of homonuclear decoupling is that it may induce some artefacts in the form of modulation and decoupling side bands in the spectrum, as well as Bloch–Siegert frequency shifts (Kupče et al., 1999). Because of the low field strength required for adiabatic decoupling ($|\gamma B_1^{max}|/2\pi = 0.7$ kHz for each ^{13}C band) and the compensating nature of the three decoupling fields, the intensity of the observed modulation side bands and the Bloch–Siegert shifts are small in the ^{13}C spectral regions of interest. The observed Bloch–Siegert shifts are close to zero for the C_6, C_8 band, and less than 20 Hz (0.1 ppm) for the $C_{1'}$ band.

The 3D ^{13}C edited TROSY-NOESY spectrum recorded on the 33-nucleotide RNA aptamer using the pulse sequence of Figure 1A including homonuclear band-selective decoupling of the C_5, $C_{2'}$, and low-field aromatic carbon bands conserves the high resolution and sensitivity achieved in the 2D ^{1}H-^{13}C correlation spectrum. With respect to a standard ^{13}C edited NOESY-HSQC experiment, the number of ambiguous assignments is considerably reduced due to ^{13}C increased resolution. On the basis of the detected NOEs between the H_6(pyrimidines) or H_8 (purines) with neighbouring $H_{1'}$ sugar protons, sequential assignment of the 33-nucleotide RNA resonances can be achieved in a straightforward way for regular RNA structure as illustrated for the example of nucleotides C30, G31, and U32 in Figure 5A. The sequential assignment pathway connecting the adjacent bases and sugars (Figure 5B) can be followed independently in the well-resolved sugar and base regions of the NOE strips extracted from the 3D spectrum. For sensitivity reasons, this was not possible for a 3D TROSY-NOESY spectrum recorded previously on a 15% ^{13}C labelled sample of the same RNA where only a small fraction of the RNA molecules in the sample contributed to the NMR signal (Brutscher et al., 1998).

These experimental results show that the line splittings in the interesting part of the ^{13}C spectrum can be removed by multiple-band-selective homonuclear decoupling. A 100% ^{13}C labelled RNA is thus clearly advantageous in terms of sensitivity compared to using partially labelled samples.

Additional base-type-selective spectral editing for application to large RNA

While TROSY-type experiments combined with homonuclear ^{13}C decoupling (or low-level ^{13}C enrichment) yield well resolved ^{1}H-^{13}C correlation spectra for the 33-nucleotide theophylline-binding aptamer, many overlapping correlation peaks are still present in the spectrum of a much larger RNA, as shown in Figure 7B for the C_6/C_8 base region of the 76 nucleotide tRNA$_3^{Lys}$. An elegant way to further simplify the NMR spectrum is the use of spectral editing filters (Otting and Wüthrich, 1990; Gemmecker et al., 1992; Dötsch et al., 1996), which exploit the different (homo- or heteronuclear) coupling topologies present in the molecule in order to suppress part of the correlation peaks or to separate the peaks in different sub-spectra. This technique reduces the complexity of the NMR spectrum and helps resolving overlaps, similar to the use of specifically isotope-labelled RNA samples. Application of spectral editing filters to high molecular weight systems, however, is generally limited by the large signal loss during the additional filter delays. As demonstrated recently for the purpose of isotopomer selection in partially ^{13}C labelled RNA, the relaxation-induced signal loss during C-C filters applied to RNA bases can be considerably reduced by TROSY-type ^{13}C spin evolution (Boisbouvier et al., 1999). A similar C-C filter sequence (Figure 1B), based on the different ^{13}C-^{13}C coupling topologies found in purine and pyrimidine bases and the distinct frequency ranges of the carbon spins (Figure 2), allows the separation of the respective NMR signals in different spectra. If the C-C filter is inserted into the pulse sequence at a point where the spin system is prepared in the slowly relaxing single-transition state C^+H^β, signal loss is substantially reduced making spectral editing a valuable tool for NMR studies of large RNAs.

Spectral editing using the C-C filter sequence of Figure 1B was first tested on the 33 nucleotide RNA aptamer for which complete ^{1}H and ^{13}C resonance assignment is available (Zimmermann et al., 1997). 2D ^{1}H-^{13}C correlation spectra recorded with either a Pyr/Pur-filter or a Cyt/Uri-filter, shown in Figure 6B and 6C, respectively, demonstrate the performance of the filter. For example, the overlapping ^{1}H-^{13}C correlation peaks of nucleotides A28 and C20 (Figures 6B1 and 6B2), and C12 and U32 (Figures 6C1

and 6C2), are resolved by these spectral editing filters. The maximal intensity observed for residual peaks in the Pyr/Pur-filter experiment (e.g. a Pyr resonance of Figure 6B1 in a Pur spectrum of Figure 6B2) is below 5% of the correctly filtered peak intensity and 8% in a Cyt/Uri-filter experiment (e.g. a Cyt resonance of Figure 6C1 in the Uri spectrum of Figure 6C2). These small artefacts, however, should not prevent the practical use of such filter sequences. The signal loss due to the additional filter delay of 15 ms is quantified experimentally for the Pyr-Pur filter (Figure 4C) and the Cyt/Uri filter (Figure 4D). The experimentally determined filter efficiency (maximal peak intensity with filter over maximal peak intensity without filter) is on average 0.70 for C_8, 0.48 for C_6, and 0.50 for $C_{1'}$ carbons for this 33 nucleotide RNA aptamer. Without additional decoupling of the low-field aromatic carbon frequency band (160±8ppm) the filter efficiency for C_8 is reduced by approximately 10%, whereas no (or only little) change is observed for C_6 and $C_{1'}$ carbons. These results can be compared to estimations based on the ^{13}C relaxation rate constants for this RNA at 18.8 T and 25 °C (Boisbouvier, 2000), yielding 0.70 for C_8, 0.57 for C_6, and 0.50 for $C_{1'}$ carbons. This shows that the C_8 and $C_{1'}$ carbons are not perturbed by the applied decoupling fields during the C-C filter, whereas the observed filter efficiency for the C_6 carbons is somewhat lower than expected theoretically. The sensitivity gain with respect to a standard (non spin-state-selective) C-C filter ranges from a factor of 1.2 for sugar carbons to about 3.3 for C_6 base carbons.

For the 33-nucleotide RNA aptamer there is little overlap in the $C_{1'}$ and base regions of the double-band-selective ^{13}C decoupled TROSY spectrum, and thus base-type-selective spectral editing is not essential for this RNA. Spectral editing, however, becomes important when studying larger RNAs as demonstrated for the 76-nucleotide $tRNA_3^{Lys}$. The base region of a multiple-band-selective ^{13}C decoupled TROSY spectrum is shown in Figure 7B. Although spectral resolution is considerably enhanced with respect to a standard HSQC (data not shown), many ^{1}H-^{13}C correlation peaks, especially for pyrimidine resonances, still overlap in this spectrum. For this particular RNA relatively few overlaps are observed between purine and pyrimidine resonances. Therefore application of a Cyt/Uri-filter proves to be most useful in resolving overlapping ^{1}H-^{13}C correlation peaks, as shown in Figures 7C and 7D. Most of the correlation peaks are resolved in the Cyt/Uri-selective TROSY spectrum.

The observed filter efficiency for $tRNA_3^{Lys}$ at 45 °C is comparable to the 33-nucleotide RNA aptamer at 25 °C. Of course the filter efficiency will decrease with increasing tumbling correlation time τ_c of the molecule, roughly proportional to $\exp(-2\delta\tau_c)$. However, while sensitivity may be increased by the use of larger amounts of RNA material or advances in NMR technology, spectral editing filters provide a simple way of increasing spectral resolution. Although signal loss during the filter is reduced by the TROSY-type ^{13}C spin evolution, application of such filters to high molecular weight systems at moderate temperature is only advantageous if sensitivity is not the most limiting factor. A 2D plane extracted from the 3D ^{13}C edited NOESY spectrum of $tRNA_3^{Lys}$ is shown in Figure 8. The cross peaks in the plotted spectral region comprise the $H_{1'}$-H_6 NOEs required for sequential assignment, as well as additional intra-nucleotide H_5-H_6 NOEs. The Cyt/Uri-filtered experiment shows several superposed NOEs in this spectral region, illustrating the importance of spectral editing techniques for NMR studies of large RNA. We believe that the experimental improvements of the 3D TROSY-NOESY experiment reported here pave the way for assigning NMR resonances of larger RNA molecules, like tRNA.

Conclusions

While the sensitivity of NMR experiments will further increase with the availability of higher field strengths and new spectrometer technology, e.g. cryoprobes, spectral resolution is not significantly effected by these technical advances. Due to the poor chemical shift dispersion in RNA new techniques for resolution enhancement and spectral simplification are required for NMR studies of biologically relevant RNA. Here we have shown that for fully ^{13}C/^{15}N labelled RNA, TROSY-type ^{13}C spin evolution combined with multiple-band-selective ^{13}C decoupling yield ^{1}H-^{13}C correlation spectra of high resolution and sensitivity. Spectral resolution can be further enhanced by the use of spectral filtering, which allows separation of ^{13}C resonances from purine and pyrimidine bases, or from cytidine and uridine bases in different spectra. TROSY-type spin evolution significantly reduces relaxation-induced signal loss, making these filters an attractive new tool for the study of large RNA whenever sensitivity is not the most limiting factor. The gain in spectral resolution obtained for ^{13}C edited

NOESY spectra proved to be very helpful for sequential resonance assignment of RNA. Extension of this methodology to other ^{13}C edited experiments of RNA is currently under investigation in our laboratory.

Acknowledgements

References

Batey, R.T., Inada, M., Kujawinski, E., Puglisi, E. and Williamson, J.D. (1992) *Nucleic Acids Res.*, **20**, 4515–4523.

Bax, A., Mehlkopf, A.F. and Smidt, J. (1979) *J. Magn. Reson.* **35**, 167–169.

Boisbouvier, J. (2000) *Thèse de l'Université Joseph Fourier*, Grenoble, France.

Boisbouvier, J., Brutscher, B., Simorre, J.-P. and Marion, D. (1999) *J. Biomol. NMR*, **14**, 241–252.

Brutscher, B. (2000) *Conc. Magn. Reson.*, **12**, 207–229.

Brutscher, B., Boisbouvier, J., Pardi, A., Marion, D. and Simorre, J.-P. (1998) *J. Am. Chem. Soc.*, **120**, 11845–11851.

Cordier, F., Dingley, A.J. and Grzesiek, S. (1999) *J. Biomol. NMR*, **13**, 175–180.

Czish, M. and Boelens, R. (1998) *J. Magn. Reson.*, **134**, 158–160.

Dieckman, T. and Feigon, J. (1997) *J. Biomol. NMR*, **9**, 259–272.

Dötsch, V., Oswald, R.E. and Wagner, G. (1996) *J. Magn. Reson.*, **B110**, 107–111.

Fiala, R., Jiang, F. and Sklenar, V. (1998) *J. Biomol. NMR*, **12**, 373–383.

Fiala, R., Czernek, J. and Sklenar, V. (2000) *J. Biomol. NMR*, **16**, 291–300.

Gemmecker, G., Olejniczak, E.T. and Fesik, S.W. (1992) *J. Magn. Reson.*, **96**, 199–204.

Kupče, E. and Freeman, R. (1996) *J. Magn. Reson.*, **A118**, 299–303.

Kupče, E., Matsuo, H. and Wagner, G. (1999) *Biol. Magn. Reson.*, **16**, 149–193.

Marino, J.P., Schwalbe, H., Anklin, C., Bermel, W., Crothers, D.M. and Griesinger, C. (1995) *J. Biomol. NMR*, **5**, 87–92.

McCoy, M.A. and Mueller, L. (1992) *J. Am. Chem. Soc.*, **114**, 2108–2112.

Nikonowicz, E.P., Michnicka, M. and Dejong, E. (1998) *J. Am. Chem. Soc.*, **120**, 3813–3814.

Nikonowicz, E.P. and Pardi, A. (1993) *J. Mol. Biol.*, **232**, 1141–1156.

Otting, G. and Wüthrich, K. (1990) *Q. Rev. Biophys.*, **23**, 39–96.

Pardi, A. and Nikonowicz, E.P. (1992) *J. Am. Chem. Soc.*, **114**, 9301–9302.

Pervushin, K., Riek, R., Wider, G. and Wüthrich, K. (1997) *Proc. Natl. Acad. Sci. USA*, **94**, 12366–12371.

Pervushin, K., Riek, R., Wider, G. and Wüthrich, K. (1998) *J. Am. Chem. Soc.*, **120**, 6394–6400.

Simorre, J.-P., Zimmermann, G.R., Mueller, L. and Pardi, A. (1996) *J. Am. Chem. Soc.*, **118**, 5317.

Simorre, J.-P., Zimmermann, G.R., Pardi, A., Farmer II, B.T. and Mueller, L. (1995) *J. Biomol. NMR*, **6**, 427–432.

Sørensen, M.D., Meissner, A. and Sørensen, O.W. (1997) *J. Biomol. NMR*, **10**, 181–186.

Tisné, C., Rigourd, M., Marquet, R., Ehresmann, C. and Dardel, F. (2000) *RNA*, **6**, 1403–1412..

Tolbert, T.J. and Williamson, J.R. (1996) *J. Am. Chem. Soc.*, **118**, 7929–7940.

Tycko, R., Pines, A. and Gluckenheimer, R. (1985) *J. Chem. Phys.*, **83**, 2775–2802.

Varani, G., Aboul-ela, F. and Allain, F.H.-T. (1996) *Progr. NMR Spectrosc.*, **29**, 51–127.

Varani, G., Aboul-ela, F., Allain, F.H.-T. and Gubser, C.C. (1995) *J. Biomol. NMR*, **5**, 315–320.

Weigelt, J. (1998) *J. Am. Chem. Soc.*, **120**, 10778–10779.

Wijmenga, S.S. and van Buren B.N.M. (1998) *Progr. NMR Spectrosc.*, **32**, 287–387.

Zhang, S. and Gorenstein, D.G. (1998) *J. Magn. Reson.*, **132**, 81–87.

Zimmermann, G.R., Jenison, R.D., Wick, C.L., Simorre, J.-P. and Pardi, A. (1997) *Nat. Struct. Biol.*, **4**, 644–649.